Surface & Coatings Technology 205 (2011) 4304–4311

Contents lists available at ScienceDirect

Surface & Coatings Technology

journal homepage: www.elsevier.com/locate/surfcoat

# Porous mullite and mullite–$ZrO_2$ granules for thermal spraying applications

E. Garcia *, J. Mesquita-Guimarães, P. Miranzo, M.I. Osendi

*Institute of Ceramics and Glass, CSIC, Madrid, Spain*

ARTICLE INFO

*Article history:*
Received 3 December 2010
Accepted in revised form 17 March 2011
Available online 12 April 2011

*Keywords:*
Thermal spraying feedstock
Spray drying
Freeze granulation
Mullite
YSZ
Coatings

ABSTRACT

Feedstock powders employed in thermal spraying applications must fulfill certain conditions in terms of particle size, morphology and homogeneity for a continuous and reliable spraying. In this work, two powder processing routes, Spray Drying (SD) and Freeze Granulation (FG), were implemented for single mullite and the equal by volume mullite/YSZ mixture. The particle size, morphology and microstructure of the agglomerated particles achieved by these two methods were studied. Free-flowing and homogeneous powders were obtained with both techniques although FG powders presented a more spherical shape and higher porosity. To evaluate the influence of the powders characteristics on the flame spraying process, both types of powders were flame sprayed under similar conditions monitoring their in-flight characteristics. The temperature reached by the particles depended mainly on their composition. Coatings were deposited on metallic substrates obtaining thicker and denser coatings with SD powders and bimodal structured coatings with FG powders.



## 1. Introduction

Thermal spraying techniques are efficient processes for producing ceramic coatings from a powdered feedstock that is injected in a flame or a plasma plume. The powders are melted and accelerated towards the substrate and the coating is formed by the controlled movement of the thermal spray gun relative to the substrate. These techniques pursue the improvement of the properties of the substrate or its protection and, consequently, they find applications in many different fields. Among others, ceramic coatings are mostly used as protective layers against wear, high temperatures and corrosive environments. In particular, the environmental barrier coatings (EBCs) have been proposed for shielding Si-based ceramics ($Si_3N_4$ and $SiC/SiC_f$) against water vapor corrosion for the next generation of gas turbines [1,2]. Diverse ceramics have been tested for EBCs and, above all, mullite stands out as a compatible layer for these Si-based ceramic components [1,3]. The inherent drawbacks of plasma sprayed mullite coatings, namely, the presence of amorphous phase that generates cracks upon crystallization and the possible volatilization of silica under high temperature steam atmospheres, have partially been overcome by the design of complex multilayered architectures with a top coat of more stable materials under vapor rich atmospheres, like $ZrO_2$–7–8 wt.% $Y_2O_3$ (YSZ), BaO—SrO—$Al_2O_3$—$SiO_2$ (BSAS) or rare earth monosilicates or disilicates [1,2,4,5]. The final properties and behavior of these EBCs under the simulated working conditions of gas turbines are conditioned by their phases, morphology and microstructure and ultimately they depend on the spraying parameters and the feedstock characteristics [6].

The thermal spraying feedstock can be found in the form of suspensions and solution precursors or, more usually, as powders. The benefits of the suspensions and solution precursors rest in the capability of achieving nanostructured coatings with improved stress compliance and reduced thermal conductivity [7]; nevertheless, it has been shown that the nanostructured-type coatings can be achieved using agglomerated fine powders as well [8]. The regular powder feedstock must fulfill stringent requirements concerning morphology and particle size to avoid clogging of the feeding systems, allow a close control of the spraying parameters and prevent flaws in the coatings [9]. The size range of these powders either as single particles or as agglomerates usually lays in the −150/+5 μm interval and the two common manufacturing methods are the fusing and crushing method and the spray-drying technique [9]. In the first, the set composition is fused, crushed and sieved to render dense and blocky shaped powders with the adequate particle size range. Conversely, in the spray drying method, a stable powder suspension is injected in the form of droplets in a heated chamber and the droplets are dried by a hot gas stream forming the agglomerated powder. This is a cost-effective and continuous operation which produces uniform and reliable powders [10]. The temperature of the process, the presence of binders, the feeding rate and the type of atomization system are some of the parameters that need to be adjusted, but the characteristics of the suspension [11,12] are also of paramount importance. All these variables affect the morphology and size of the final agglomerates. The spherical morphology and a correct particle size distribution for an even flow of the particles through the particular thermal spray system can be achieved in this way [13]. Furthermore, spray-dried (SD)

* Corresponding author. Tel.: +34 91 735 58 40; fax: +34 91 735 58 43.
*E-mail address:* garcia@icv.csic.es (E. Garcia).

0257-8972/$ – see front matter © 2011 Elsevier B.V. All rights reserved.
doi:10.1016/j.surfcoat.2011.03.060

powders should exhibit enough cohesion to withstand the turbulence of the thermal spray jet without breaking apart. If the spray-dried powders are too fine and porous (low cohesive strength) they do not exhibit the enough inertia required to cross the streamlines of the spray jet, being projected to its periphery without depositing onto the substrate. They may also evaporate by superheating before splashing on the substrate, resulting in a poor deposition efficiency and weak bonding [14].

Although spray drying has proved to be an efficient technique for producing porous granules, it also has some drawbacks. For example, the scale of the atomizers required to get particles in the −150/+5 μm size range is usually quite large as the diameter of the particles is mostly affected by the size of the drying chamber [10]. Problems may also arise regarding the granule homogeneity, since the drying step under the hot gas/air stream favors liquid migration within the granules, which may cause some segregation of the binder and smaller particles to the periphery of the drop, thus giving inhomogeneous granules. Although these issues can be minimized with a good homogenization and stabilization of the original suspension, alternative methods based on the freeze-drying of suspensions have been developed [15–20]. In this technique, the suspension is rapidly frozen and, afterwards, dried by lyophilization. Freeze-drying is a method extensively used in the drug industry [15] to process bulk products in the form of powder cakes, with the aim of avoiding concentration gradients and the degradation of biological material by the rise of temperature required for SD methods. The freeze-dying process was used to get $Al_2O_3$/SiC composite powders feedstock from a dispersion of the corresponding nanopowders, nevertheless particles had a wide size distribution, a large fraction of fine sizes and, consequently, poor flowability [16]. Therefore, for achieving thoroughly sprayable powders this route should be improved by including a granulation step; in particular, we propose a freeze granulation (FG) step that consists on spraying a powder suspension into a chilled vessel controlling the drop size. The drops (granules) are instantaneously frozen and, then, the collected frozen granules are dried by ice sublimation to avoid any segregation. FG method has been employed in the pharmaceutical industry to get advantage of the rapid freezing of the particles in terms of size and dispersion of constituents, obtaining, after lyophilization, a product with rapid dissolution properties [17,18]. Other field of application of this technique is the food processing industry where dry flowable products with better quality than those obtained from spray drying have been produced [19,20].

Freeze granulation method has also been used in the production of free-flowing spherical shaped ceramic powders to get quite uniform distribution of pressing aids and sintering additives [21–27] and for processing catalysts of higher surface area [28] as well. Present authors attested for the first time the employ of this technique [29] to get particles of a size suitable for thermal spraying (−150/+5 μm), with a rather good yield and using quite cheap and compact equipment. A main advantage of this FG route was that the particle size distribution could be easily tuned by changing the size of the spraying nozzle. Therefore, FG is very flexible as it can render laboratory scale batches of cutting-edge compositions or even industrial scale amounts of thermal spray powders.

The principal aim of present work is to study the suitability of spray drying and freeze drying methods for granulation of fine ceramic powders, in particular, mullite and mullite/$ZrO_2$ composites, to make them suitable for thermal spraying systems. The granules of mullite and the equal by volume mulite/$ZrO_2$ composition were characterized regarding their size distribution, homogeneity, density and flowability. The temperature and velocity of the in-flight particles were studied for the different powder batches with the aid of an oxy-acetylene flame spraying equipment using a diagnostic system. Finally, the characteristics of the diverse coatings built under the same spraying conditions were also studied and related to the particular features of each feedstock.

## 2. Experimental

Commercial powders of mullite ($3Al_2O_3 \cdot 2SiO_2$) and zirconia ($ZrO_2$) stabilized with 7 wt.% $Y_2O_3$ (YSZ) were the starting materials. Mullite powders (Baikalox SASM, Baikowski Chemie, Annecy, France) containing 1.8 wt.% of free $SiO_2$ and less than 0.2 wt.% of impurities and with average particle size of 1.3 μm, and YSZ powders (TZ4Y, Tosoh, Tokyo, Japan), 99.95% pure and with an average particle size of 0.3 μm, were used as starting powders. Aqueous suspensions of mullite and 50 vol.% mullite-50 vol.% YSZ composition, labeled as mullite/$ZrO_2$, both at two different solid contents, 30 and 50 wt.%, were prepared. To get stable powder slurries, a polyelectrolyte dispersant (Dolapix CE 64 CA, Zschimmer-Schwarz, Germany) was added to the water dispersion media while stirring and, next, powders were slowly added. Subsequently, to provoke the thoroughly mixing of dispersant and powders and avoid agglomeration, continuous attrition milling was performed at a rate of 1 h per liter of suspension. A polysaccharide preparation (KB 1247, Zschimmer-Schwarz, Germany) was selected as the binder agent due to its superior cohesive strength and the lack of residues after burning. It was added in a 5 wt.% referred to the solid content of the suspension and additional stirring was performed. The viscosity of the suspension was determined with a rehometer (CVO 100 D, Bohlin Instruments, UK) for various dispersant contents.

The slurries were spray-dried with a rotary atomizer spray drying system (Mobile Minor Spray Dryer, basic model, Niro Atomizer, Søborg, Denmark) in a co-current flow. The inlet temperature ranged from 300 to 350 °C and the temperature at the exit of the spray dryer varied from 100 to 150 °C. The slurry feed rate was 65 ml $min^{-1}$, at $3 \cdot 10^5$ Pa of air pressure.

For the freeze granulation step, an in-house made system was built that consisted of a suspension feeding system, an air nozzle for droplet generation and a collecting vessel containing the frozen media. The feeding system was a peristaltic pump that delivered the slurry at a rate of 65 ml $min^{-1}$ through an air atomizing nozzle provided with two orifices for the fluid and air, respectively. The atomizing gas pressure was $4 \cdot 10^5$ Pa. The air sprayed mix was projected into the vessel containing liquid nitrogen. Then, the frozen granules were removed from the freezing media and refrigerated at −24 °C before being transferred to the freeze-drier (Freezone Plus 12L, Labconco Corp. USA) to sublimate the ice. The freeze dryer had heated trays that allowed processing large amounts of frozen granules and the control of the tray temperature. After drying, granules were sorted through sieving to get the required size distribution.

A heat treatment at 120 °C was done for both spray dried and freeze granulated powders to promote gelation and crosslinking in the binder [30]. For the FG powder, half an hour of heating at 1500 and 1250 °C for mullite and mullite/$ZrO_2$ powders, respectively, was done to enhance the particle cohesion, based on the known sintering kinetics of mullite and mullite/$ZrO_2$ powders [31].

Particle size distributions of the final SD and FG batches were determined with a laser diffraction particle size analyzer (Mastersizer S, Malvern, United Kingdom). The powders bulk density ($\rho_{bulk}$) was measured by weighting the mass of powder filling a container of fixed volume (100 ml). Next the container was vibrated up to the point where the powders volume change was below 2% variation, then calculating the powder tapped density ($\rho_{tap}$). The ratio $\rho_{tap}/\rho_{bulk}$, known as the Hausner ratio, serves to rapidly evaluate the packing and flowability of a particular powder, where a Hausner ratio closer to 1 means a better flow performance [32]. Some particles of SD and FG feedstocks were mounted in epoxy resin and polished using diamond compounds for microstructural observation.

Both powder batches were flame-sprayed onto metallic substrates using an oxygen–acetylene gun (model CastoDyn DS 8000, Eutectic Castolin, Spain). The torch input power was 28 kW, the acetylene/oxygen volumetric flow ratio was that of the stoichiometric mixture and the oxygen and acetylene pressures were $4 \cdot 10^5$ and $7 \cdot 10^4$ Pa,

**Table 1**
Feed rate, average agglomerate size ($d_{50}$), bulk density ($\rho_{bulk}$), tap density ($\rho_{tap}$) and Hausner ratio ($H_r = \rho_{tap}/\rho_{bulk}$) of the different processed powders.

| | Feed rate kg $h^{-1}$ | $d_{50}$ (μm) | $\rho_{bulk}$ (g $cm^{-3}$) | $\rho_{tap}$ (g $cm^{-3}$) | $H_r$ |
|---|---|---|---|---|---|
| Mullite SD | 0.7 | 26 | 0.64 | 0.8 | 1.25 |
| Mullite FG | 1.5 | 81 | 0.45 | 0.53 | 1.18 |
| Mullite/$ZrO_2$ SD | 2.8 | 23 | 1.1 | 1.27 | 1.15 |
| Mullite/$ZrO_2$ FG | 1.6 | 77 | 0.55 | 0.61 | 1.11 |

respectively. The powder feed rate was governed by the choice of diaphragm diameter in the powder module, 1.5 mm for all cases, which gave the feed rates shown in Table 1. A stand-off distance of 150 mm was selected to avoid the overheating of the metallic substrates. Single splats were collected by quickly passing a mirror polished stainless steel substrate in front of the torch at the set stand-off distance. The in-flight particle state (particle velocity and temperature) at that distance was measured with the Accuraspray g-3 (Tecnar Automation, St-Bruno, QC, Canada) diagnostic system. Low magnification views of the FG and SD agglomerated particles and the corresponding collected splats were obtained with a table top scanning electron microscope (SEM) (TM1000, Carl-Zeiss, Germany). The higher magnification top views and the polished crossed sections of the different coatings were observed in the SEM (DMS-950 Carl-Zeiss, Germany). Elemental mappings for Al (K), Si (K) and Zr (L) in the composite granules were obtained with the X-ray energy dispersive spectroscopy analysis system (EDS, Tracor Northern) attached to the scanning electron microscope. X-ray diffraction analyses (XRD) were performed on the coating surface using an Xpert PRO diffractometer (PANalytical, Netherlands) with a θ/2θ configuration, in the 15–55° 2θ range, with a step of 0.0165 and a time per step of 50 s.

## 3. Results and discussion

Shear stress vs. shear rate curves of the different dispersions showed a linear (Newtonian) behavior. The suspension viscosity as a function of the amount of dispersant was determined at a shear rate of 380 $s^{-1}$ (Fig. 1). Whereas the viscosity of the mullite slurries was rather low and scarcely affected by solid and dispersant contents, mullite/$ZrO_2$ slips presented higher viscosity values, which were dependent on the solid content. At least 0.4 wt.% of dispersant was needed to achieve viscosity levels similar to those of the mullite suspensions. This behavior can be explained by the surface charge (zeta potential) of the mullite and YSZ powders at the natural pH of these suspensions. The reported isolectric point of same mullite powders occurred at pH = 6.5 [33] and that of similar $ZrO_2$ powders stabilized with 3 mol% $Y_2O_3$ was at pH = 8 [34]. At the natural pH of the mullite slurry (7.7), a zeta potential value of −15 mV has been

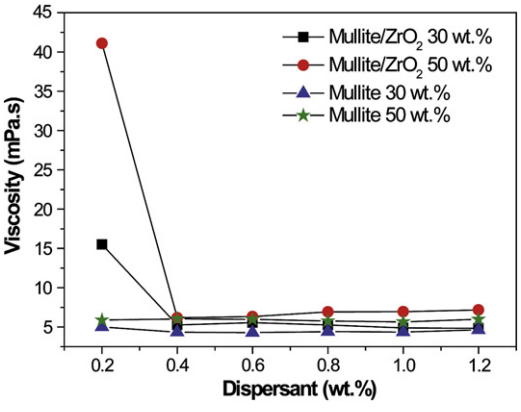


**Fig. 1.** Viscosity of the mullite and mullite/$ZrO_2$ suspensions as a function of the dispersant concentration for 30 and 50 wt.% solid contents.

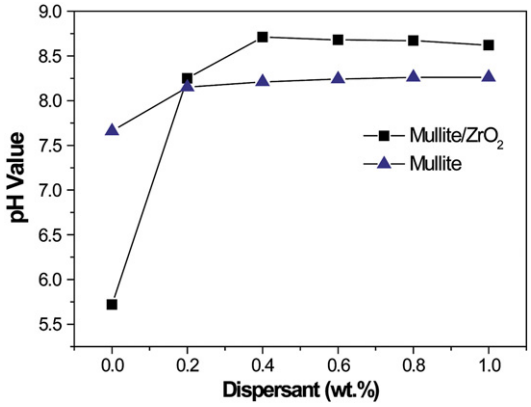


**Fig. 2.** Evolution of the pH of the mullite and mullite/$ZrO_2$ suspensions (30 wt.% of solid content) as a function of the concentration of polyectrolyte dispersant.

reported [33], whereas the addition of the polyelectrolyte moves the suspensions pH to more basic values leveling off at pH = 8 for a concentration of 0.2% of polyelectrolyte (Fig. 2), thus giving zeta potentials in the range of −30 mV [33] that would explain the low viscosity of the mullite suspensions. On the other hand, the natural pH of mullite/$ZrO_2$ slurries was about 6 (Fig. 2), which is very close to the isoelectric point of mullite and justifies the higher viscosity of the mullite/$ZrO_2$ slurry. However, for polyelectrolyte contents above 0.4 wt.%, the pH of the mullite/$ZrO_2$ slurry raised up to 8.5 (Fig. 2), where zeta potential values of mullite and YSZ suspensions are −35 mV [33,34], which would give stable suspensions and decrease viscosity as observed. Further increase in the dispersant concentration did not produce any changes in the viscosity of these suspensions in consonance with the constant pH. Considering that for dispersant contents ≥0.4 wt.% the viscosity is similar for every suspension and, on the other hand, the propensity of the spray dried granules to form craters when increasing the dispersant content [11,35], the concentration of 0.4 wt.% of polyelectrolyte was chosen to assure low viscosity and stability of suspensions during handling.

The particle size distributions of mullite and mullite/$ZrO_2$ feedstocks for both agglomeration routes are plotted in Fig. 3 exhibiting monomodal distributions in both cases. For FG batches, the measurement corresponded to the −150/+32 μm powder fraction, selected through sieving. The particles above 150 μm (19% of the collected batch) where discarded for being outside of the sprayable size span and the smaller fraction of particles below 32 μm (11%) were eliminated to get a narrower size distribution. The particle range selected amounted 70% of the initial quantity. The average particle sizes ($d_{50}$) achieved for each route and composition are shown in Table 1; the values of bulk and tap densities are given in the table as well. As it can be seen, mullite

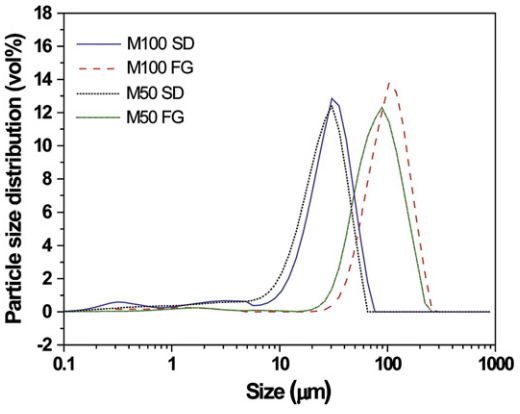


**Fig. 3.** Particle size distributions for Spray Dried (SD) and Freeze Granulated (FG) powders.

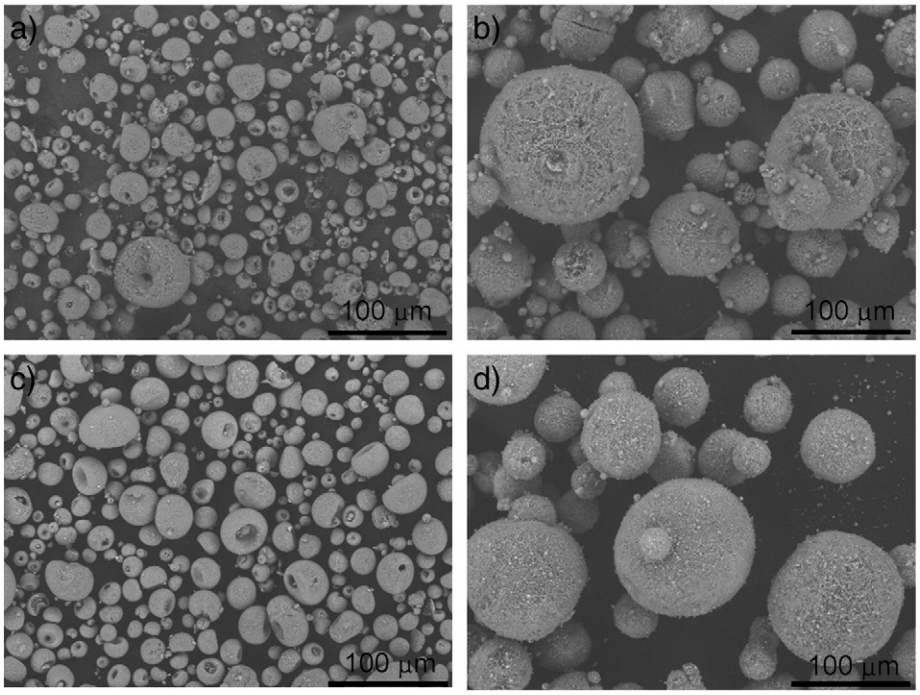


**Fig. 4.** Scanning electron microphotographs of the, a) mullite SD, b) mullite FG, c) mullite/$ZrO_2$ SD and d) mullite/$ZrO_2$ FG.

particles always showed slightly bigger sizes than the analogous mullite/$ZrO_2$ composite powders. This situation is probably due to the more compact self-arrangement of mullite and $ZrO_2$ powders in the suspension due to the combination of electrostatic and steric forces acting on their surfaces. The widths of the distributions were ~30 and 100 μm for SD and FG powders, respectively, independently of the composition. The bulk density of both types of mullite/$ZrO_2$ granules was clearly higher than the bulk density of the corresponding mullite powders. The tap density of the composite powders was closer to their bulk density driving to Hansher ratios nearer to 1, indicating a better flowability of these composite powders that of mullite ones, which also explains the higher powder feed rates during flame spraying for the composite powders (Table 1). Comparing the two granulation methods for the same composition, we can say that flowability was higher for FG than for SD feedstock.

The SD and FG granules were mainly rounded except for some dome-shaped granules in SD batches (Fig. 4a and c), which are typically formed in SD powders. Conversely, FG granules showed an even spherical aspect (Fig. 4b and d). Images of the polished cross section of the above particles showed again the typical inner cavity for many of the SD particles (Fig. 5a and c) but quite different features for FG particles. In these, it is interesting to note a certain segregation in porosity, especially

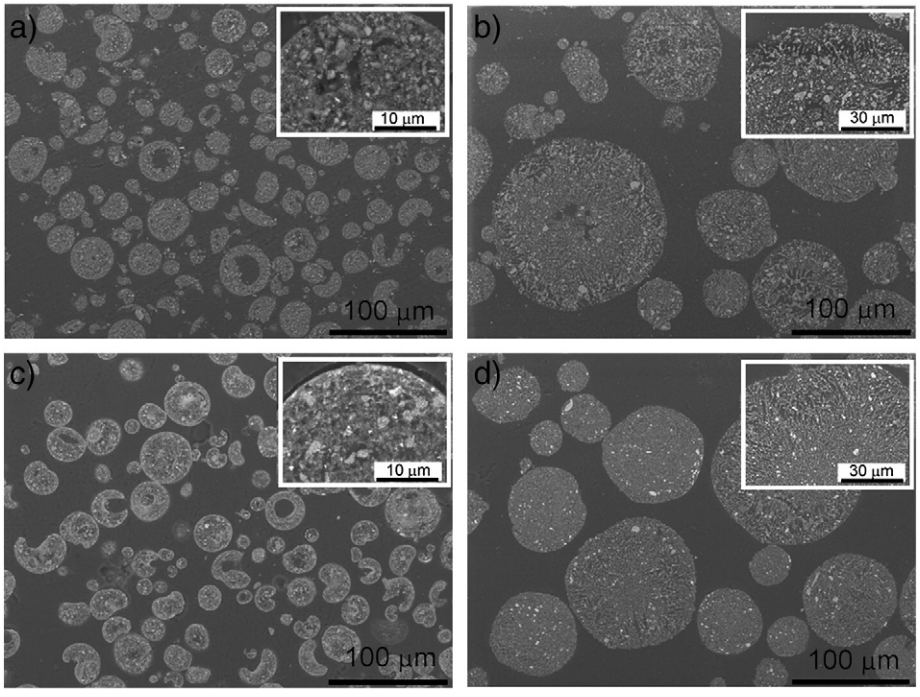


**Fig. 5.** Scanning electron cross-sectional views of a) mullite SD, b) mullite FG, c) mullite/$ZrO_2$ SD and d) mullite/$ZrO_2$ FG. Higher magnification details of each powder are also shown.

for larger particles >100 μm (Fig. 5b and d), and even more evident for those of single mullite where larger size pores were definitely observed at the particle rim (Fig. 5b). This characteristic played an important effect on the temperature that particles achieved in the flame, as will be shown later. EDS mappings for Zr, Si and Al elements carried out on polished cross-section of SD (Fig. 6a) and FG (Fig. 6b) composite granules showed a quite homogeneous distribution of these elements for both types of processes. Therefore, no evidence of phase segregation occurred for any of the processing routes.

The temperature (T) and velocity (V) of the particles during flame spaying are shown in Table 2. The temperatures of the different powders were quite high for a flame spraying arrangement, considering that the adiabatic flame temperature calculated for the present experimental conditions was 3100 °C [36]. These temperatures are well above the complete melting temperatures of mullite (~1860 °C) [37] and the mullite/$ZrO_2$ composition (~2200 °C) [38]. Despite the similar in-flight velocities of the particles, the temperatures were always lower for the mullite/$ZrO_2$ granules than for the single mullite powders, independently of their SD or FG morphology.

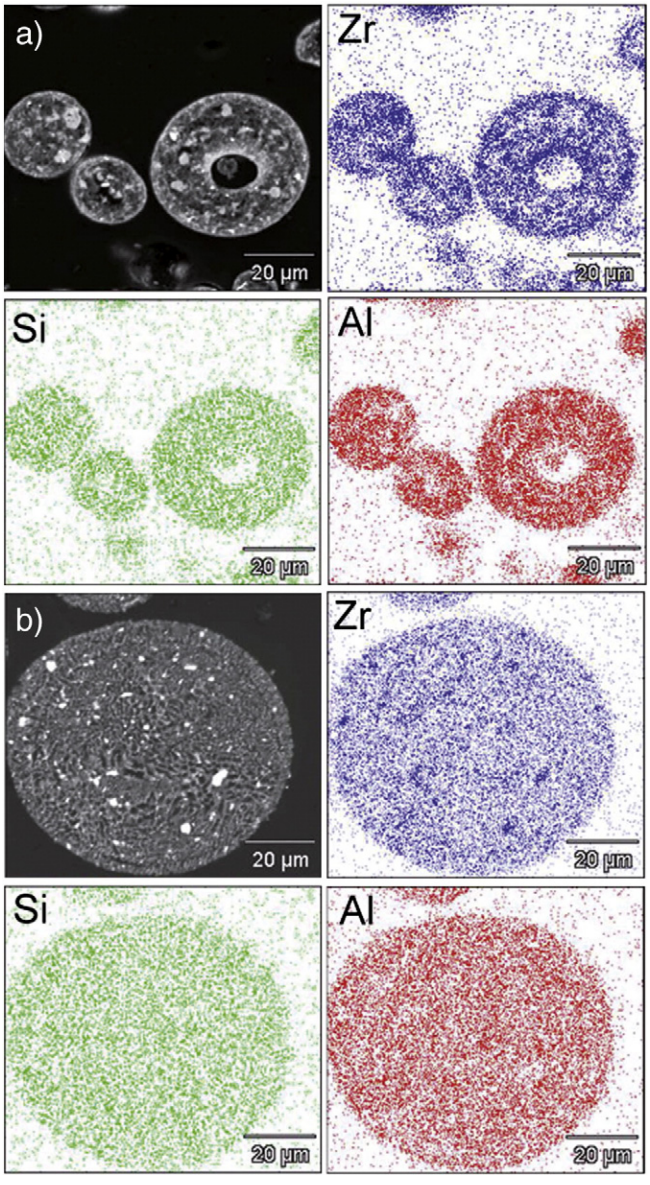


**Fig. 6.** EDS elemental mappings for Zr, Si and Al in individual granules of a) SD and b) FG mullite/$ZrO_2$ powders.

**Table 2**
Velocity and temperature of the flame sprayed powders recorded at 150 mm of stand-off distance.

| | V ($m \cdot s^{-1}$) | T (°C) |
|---|---|---|
| Mullite SD | 56 ± 1 | 3326 ± 36 |
| Mullite FG | 51 ± 1 | 3486 ± 17 |
| Mullite/$ZrO_2$ SD | 50 ± 1 | 3083 ± 18 |
| Mullite/$ZrO_2$ FG | 60 ± 1 | 3022 ± 10 |

In this way, differences in measured temperature must be explained by the compositional differences. It can be assumed that agglomerates with similar diameter, shape and porosity absorb the same amount of heat during flight. Thus, the relative increment of temperature can be estimated using the expression:

$$\Delta T_m / \Delta T_{mz} = C_{mz}\rho_{mz} / C_m\rho_m \quad (1)$$

where, C is the specific heat and ρ is the theoretical density of mullite (m) and the mullite/$ZrO_2$ (mz) composite, respectively. Eq. (1) predicts a value of 1.09 for the $\Delta T_m/\Delta T_{mz}$, which indicates that mullite particles will reach higher temperature than the mullite/$ZrO_2$ particles. From the measured temperatures shown in Table 2, $\Delta T_m/\Delta T_{mz}$ values of 1.08 and 1.15 are obtained for SD and FG powders, respectively; that is, the temperature ratio is very close to the predicted in the case of SD powders but slightly higher for FG powders. These higher temperatures of FG feedstocks can be explained by differences in heat propagation within the granules. In fact, the graded porosity observed in FG powders (details in Fig. 5b and d), with bigger pores at the particle rim, most probably hindered heat flow towards the particle core. In this way, the temperature at the particle surface would rise above that of SD particles that had smaller size and homogenously distributed pores (details in Fig. 5a and c).

Single splats collected for the SD and FG powders are shown in Fig. 7. SD powders formed well melted splats of quite regular shape (Fig. 7a and c) whereas the splats from the FG powders were larger and more irregular (Fig. 7b and d), independently of composition. The empty areas in the FG mullite splats were probably created by the bouncing back of matter that did not melt totally during their flight due to both the bigger size and higher porosity of the particles. The presence of small melted zones surrounding the main splat (pointed by arrows in Fig. 7) is usually associated to satellite drops developed by the splashing of the melted particles upon their impact on the cold substrate or the shrinkage of overheated particles during cooling on the substrate [9]. In the case of the big FG granules, these features can be related to the explosion of some particles as well. Some spherical pores were also observed in the splats of both SD and FG mullite/$ZrO_2$, produced by the gas entrapment during the rapid solidification of the melted particles[39], this was more obvious for the mullite/$ZrO_2$ composite particles probably due to differences in liquidus temperature, viscosity and liquid-gas interfacial energy.

The top views of the coatings (Fig. 8) show features that correlate well with the characteristics seen for single splats, confirming larger size splats for FG coatings and a mixture of melted and unmelted particles (Fig. 8b and d), whereas the SD coatings were built-up of well melted particles (Fig. 8a and c), The unmelted particles seen at the top surface of the FG mullite coating (Fig. 8b) were reminiscent of the original FG agglomerates, which did not stay enough time in the flame hot section to melt completely. The cross-sectional views of these coatings evidenced the different thickness of SD (Fig. 9a and c) and FG coatings (Fig. 9b and d) under the reported thermal spraying conditions. The coating thickness is obviously linked to the number of melted particles that were able to reach and pile-up on the substrate and, therefore, it can be related with the deposition efficiency, which depends on feedstock flow rate and the particle density and size, for the specific thermal energy developed by the projection technique [6,9]. Similar thickness was obtained with both single mullite

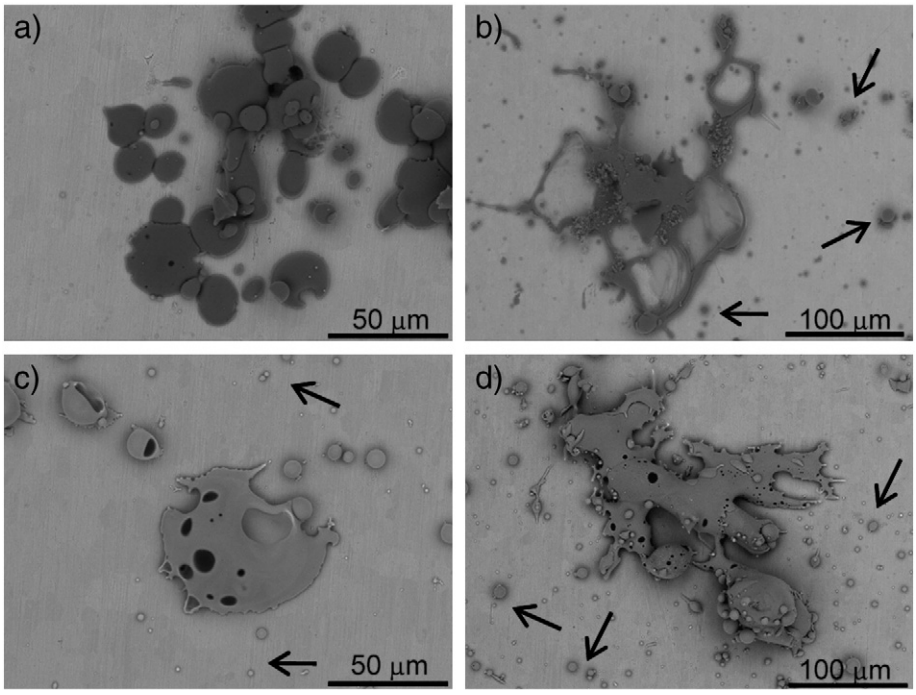


**Fig. 7.** Morphology of the splats recorded for the different powders, a) mullite SD, b) mullite FG, c) mullite/$ZrO_2$ SD and d) mullite/$ZrO_2$ FG. Arrows show the satellite melted drops.

powders (Fig. 9a and b) although higher feed rate was measured for the FG than for SD powders. The lower deposition efficiency of FG powders can be produced by either the bouncing back of unmelted particles from the substrate or the vaporization of the small particles coming from the disintegration of poorly cohered agglomerates. In the case of the composite particles, the coating thickness produced from SD feedstock (Fig. 9c) was almost double than that obtained from FG (Fig. 9d) in agreement to the lower feeding rate of the last (Table 1).

The detailed observation of the coating microstructures revealed additional interesting features for FG feedstocks. The unmelted FG particles resembling the original agglomerates are formed by a porous poorly sintered core surrounded by a denser melted rim (Figs. 9 and 10), which seems thicker for mullite/$ZrO_2$ than for mullite coatings. As the large particle size and high porosity of FG particles would probably have limited heat flow within the granules, the melting chiefly would occur at the rim of the larger particles while the core would remain unmelted, as experimentally seen. For the mullite/$ZrO_2$ composition, the comparatively lower liquidus temperature (1750 °C) [38] would drive heat flow inside the granule giving a thicker rim compared to pure FG mullite coating, as observed (Fig. 10). The thinner particle rim overheated in the case of FG mullite can therefore justify the higher in-flight temperature measured for these particles (Table 2). It is

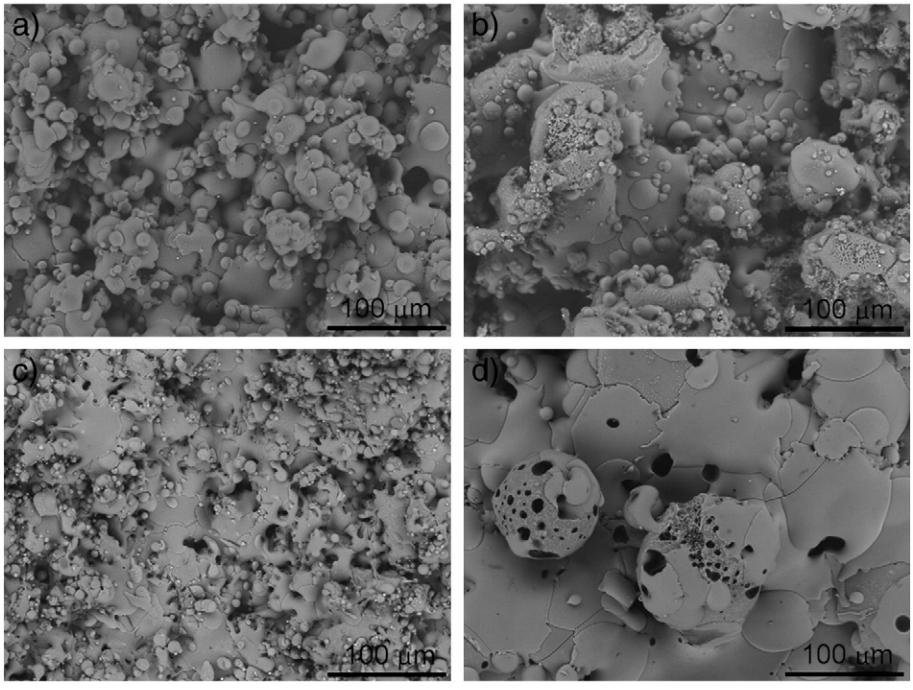


**Fig. 8.** SEM top view micrographs of the a) mullite SD, b) mullite FG, c) mullite/$ZrO_2$ SD and d) mullite/$ZrO_2$ FG coatings.

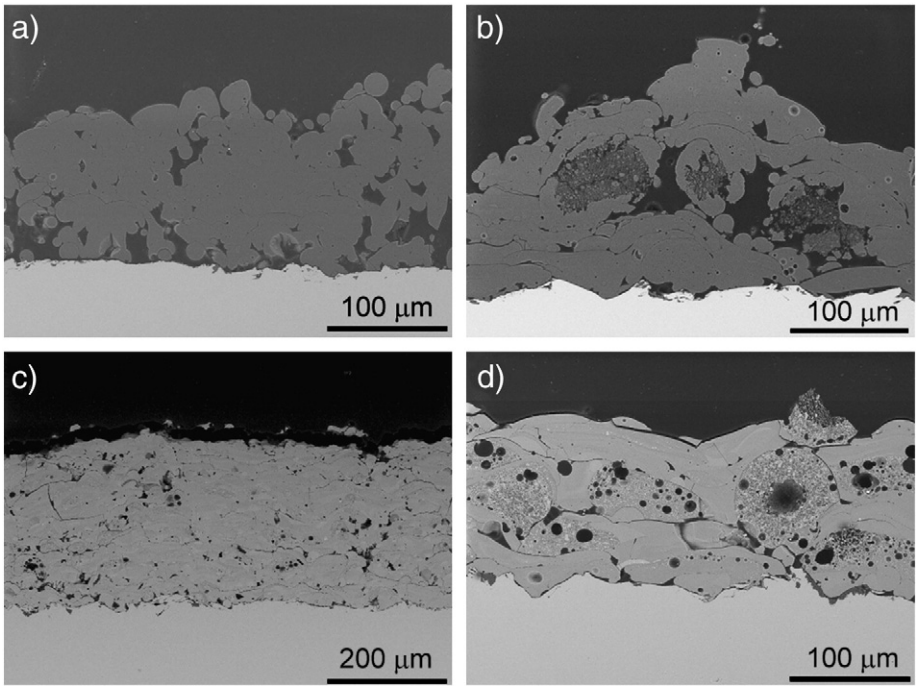


**Fig. 9.** SEM micrographs of the polished cross section of the a) mullite SD, b) mullite FG, c) mullite/$ZrO_2$ SD and d) mullite/$ZrO_2$ FG coatings.

noteworthy to point out the exceptional microstructure of FG coatings showing a combination of melted areas surrounding submicronic porous zones, resembling that of bimodal nanostructured coatings [40] developed from nanosized powders.

The X-ray diffraction patterns of the SD and FG original powders and coatings are shown in Fig. 11. The well defined peaks detected in the original powders demonstrate that they were fully crystalline. In the case of mullite powders (Fig. 11a) only mullite and one small peak associated with free $SiO_2$ were detected. The pattern of the composite powders showed the characteristics peaks of mullite and tetragonal $ZrO_2$ (t-$ZrO_2$), although a peak of residual monoclinic $ZrO_2$ (m-$ZrO_2$) was detected as well. The SD mullite coating (see Fig. 11a) was totally amorphous and the mullite FG coating (Fig. 11a) showed well defined mullite diffraction peaks, superimposed to an amorphous background, indicating the coexistence of melted and unmelted particles, as pointed by the SEM observations (Fig. 9b). The XRD patterns of both mullite/$ZrO_2$ coatings (Fig. 11b) showed the presence of t-$ZrO_2$, whereas a hump, associated with the presence amorphous phase and mullite peaks in the FG coating were also appreciable. The broad diffraction peak in the SD mullite/$ZrO_2$ coating was associated with the small particle size of t-$ZrO_2$ resulting from the rapid crystallization of the melted droplets, whereas mullite peaks and the width of the t-$ZrO_2$ diffraction peak (Fig. 11b) pointed out the presence of unmelted particles in the FG mullite/$ZrO_2$ coating (Fig. 9d).

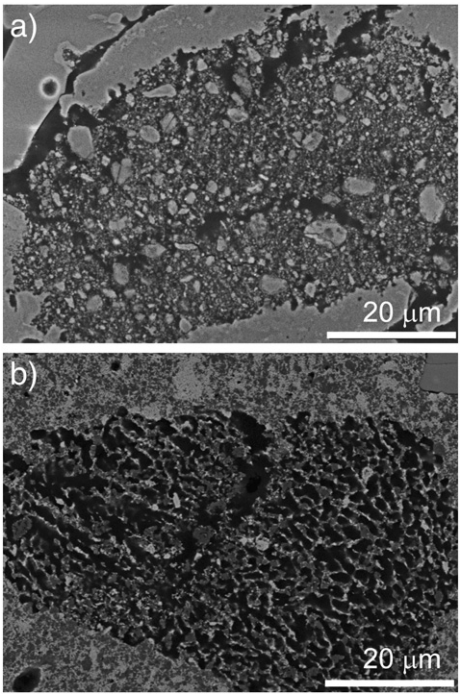


**Fig. 10.** SEM details of unmelted FG granules in a) mullite and b) mullite/$ZrO_2$ FG coatings.

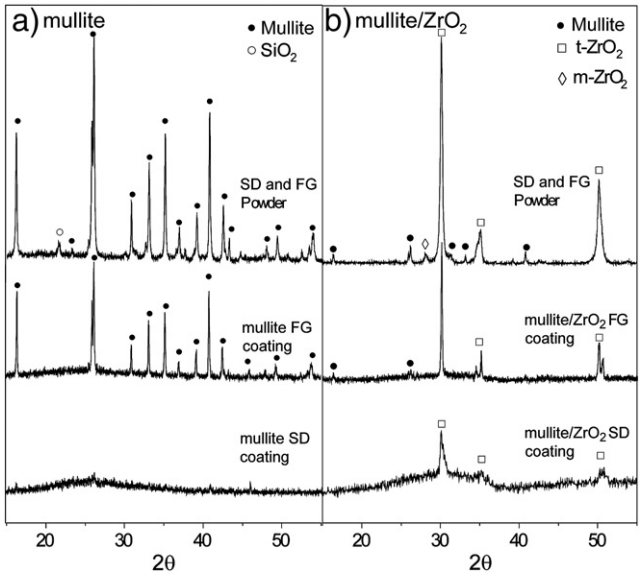


**Fig. 11.** Patterns of SD and FG feedstock powders and coatings for a) mullite and b) mullite/$ZrO_2$ compositions.

The retained crystallinity in the FG coatings would probably limit the volume changes due to mullite crystallization upon heating and hence extensive cracking.

## 4. Conclusions

Sprayable powders of mullite and mullite–$ZrO_2$ were prepared from homogeneous suspensions, after drying and agglomeration by either spray drying (SD) or freeze granulation (FG) methods. Both powders were adequate feedstock for thermal spraying techniques regarding size and flowability. The FG process had an inherent feasibility for producing a wider size range of monomodal particles using compact and cheap equipment. It has been proved that the in-flight temperature achieved by the granules depended mainly on their composition (specific heat and theoretical density), being at least 250 °C higher for mullite than for mullite/$ZrO_2$ particles. A temperature gradient within the FG granules was inferred following their porosity gradient. Accordingly, FG and SD coatings had quite different microstructures, SD particles gave thicker and denser coatings while FG coatings had a unique bimodal microstructure, which combined melted and submicronic porous areas.

## Acknowledgments

This work was supported by NRC-CSIC program (project 2007CA003). Additional financial support of MICINN (Ministry of Science and Innovation, Spain) under project MAT2009-09600 is also recognized. E. Garcia acknowledges the Ramón y Cajal Program (MICINN) for the financial support.

## References

[1] S. Ueno, D.D. Jayaseelan, T. Ohji, Int. J. Appl. Ceram. Technol. 1 (2004) 362.
[2] N. Miriyala, J. Kimmei, J. Price, K. More, P. Tortorelli, H. Eaton, G. Linsey, E. Sun, Proceedings of ASME TURBO EXPO 2002 June 3–6, ASME, Amsterdam, The Netherlands, 2002, p. 1.
[3] R. Krishnamurthy, B.W. Sheldon, J.A. Haynes, J. Am. Ceram. Soc. 88 (2005) 1099.
[4] E. Garcia, J. Mesquita-Guimarães, P. Miranzo, M.I. Osendi, C.V. Cojocaru, Y. Wang, C. Moreau, R.S. Lima, J. Therm. Spray Technol. 20 (2011) 83.
[5] K.L. More, P.F. Tortorelli, L.R. Walter, J.B. Kimmel, N. Miriyala, J.R. Price, E.Y. Sun, G.D. Linsey, ASME paper 2002-GT-30630. IGTI 4 A, 2002, p. 155.
[6] P. Fauchais, G. Montavon, G. Bertrand, J. Therm. Spray Technol. 19 (2009) 56.
[7] N.P. Padture, K.W. Schlichting, T. Bhatia, A. Ozturk, B. Cetegens, S. Jiang, T.D. Xiao, P.R. Strutt, E. García, P. Miranzo, M.I. Osendi, Acta Mater. 49 (2001) 2251.
[8] R.S. Lima, B.R. Marple, J. Therm Spray Technol. 16 (2007) 1640.
[9] J.R. Davis (Ed.), Handbook of Thermal Spray Technology, ASM International, Materials Park, OH, 2004.
[10] S.J. Lukasiewicz, J. Am. Ceram. Soc. 72 (1989) 617.
[11] W.J. Walker Jr., J.S. Reed, S.K. Verma, J. Am. Ceram. Soc. 82 (1999) 1711.
[12] G. Bertrand, P. Roy, C. Filiatre, C. Coddet, Chem. Eng. Sci. 60 (2005) 95.
[13] V. Viswanathan, K.E. Rea, A. Vaidya, S. Sealw, J. Am. Ceram. Soc. 91 (2008) 379.
[14] X.Q. Cao, R. Vassen, S. Schwartz, W. Jungen, F. Tietz, D. Stöever, J. Eur. Ceram. Soc. 20 (2000) 2433.
[15] X. Tang, M.J. Pikal, Pharm. Res. 21 (2004) 191.
[16] S. Jiansirisomboon, K.J.D. MacKenzie, S.G. Roberts, P.S. Grant, J. Eur. Ceram. Soc. 23 (2003) 961.
[17] H. Leuenberger, J. Nanopart. Res. 4 (2002) 111.
[18] T.L. Rogers, A.C. Nelsen, J. Hu, J.N. Brown, M. Sarkari, T.J. Young, K.P. Johnston, R.O. Williams III, Eur. J. Pharm. Biopharm. 54 (2002) 271.
[19] C.S. MacLeod, J.A. McKittrick, J.P. Hindmarsh, M.L. Johns, D.I. Wilson, J. Food Eng. 74 (2006) 451.
[20] J.P. Hindmarsh, A.B. Russell, X.D. Chen, J. Food Eng. 78 (2007) 136.
[21] S.M. Olhero, I. Ganesh, P.M.C. Torres, F.J. Alves, J.M.F. Ferreira, J. Am. Ceram. Soc. 92 (2009) 9.
[22] I. Ganesh, G. Sundararajan, S.M. Olhero, P.M.C. Torres, J.M.F. Ferreira, Ceram. Int. 36 (2010) 1357.
[23] T. Moritz, A. Nagy, J. Nanopart. Res. 4 (2002) 439.
[24] N. Uchida, T. Hiranami, S. Tanaka, K. Uematsu, Am. Ceram. Soc. Bull. 81 (2002) 57.
[25] T. Moritz, T. Reetz, CFI-Ceram. Forum Int. 70 (1993) 168.
[26] B. Nyberg, E. Carlström, R. Carlsson, in: G. Ziegler, H. Hausner (Eds.), Basic Science and Processing of Ceramics, Euro-Ceramics II, vol. 1, Deutsche Keramische Gesellschaft, 1993, p. 447.
[27] E. Linden, E. Carlström, L. Eklund, B. Nyberg, R. Carlsson, J. Am. Ceram. Soc. 78 (1995) 1761.
[28] S.H. Lee, J.Y. Lee, Y.M. Park, J.H. Wee, K.Y. Lee, Catal. Today 117 (2006) 376.
[29] E. Garcia, J. Mesquita-Guimarães, P. Miranzo, and M.I. Osendi, Procedure for obtaining ceramic feedstock for thermal spraying applications, Patent 2009, ICV-CSIC, Ref. ES1641.581, Spain.
[30] J.S. Reed, Principles of Ceramic Processing, John Wiley & Sons, Inc, New York, 1995.
[31] J.S. Moya, M.I. Osendi, J. Mater. Sci. Lett. 2 (1983) 599.
[32] P.O. Grey, J.K. Beddow, Powder Technol. 2 (1968) 121.
[33] R. Barea, M.I. Osendi, J.M.F. Ferreira, P. Miranzo, J. Am. Ceram. Soc. 88 (2005) 777.
[34] E. López-López, C. Baudín, R. Moreno, Int. J. Appl. Ceram. Technol. 5 (2008) 394.
[35] A. Tsetskou, C. Agrafiotis, I. Leon, A. Milias, J. Eur. Ceram. Soc. 21 (2001) 493.
[36] C. Cano, M. Belmonte, M.I. Osendi, P. Miranzo, Surf. Coat. Technol. 201 (2007) 3307.
[37] H. Schneider, K. Okada, J.A. Pask, Mullite and Mullite Ceramics, John Wiley & Sons, NY, 1994.
[38] M.C. Greca, J. Emiliano, M.A. Segadães, J. Eur. Ceram. Soc. 9 (1992) 271.
[39] M.A. Sainz, M.I. Osendi, P. Miranzo, Surf. Coat. Technol. 202 (2008) 1712.
[40] R.S. Lima, B.R. Marple, J. Therm. Spray Technol. 17 (2008) 846.